Shape Changes in AuPd Alloy Nanoparticles Controlled by Anisotropic Surface Stress Relaxation

Diana Nelli,[†] Cesare Roncaglia,[†] Riccardo Ferrando,[*,‡,§] and Chloé Minnai[*,¶,§]

[†]*Dipartimento di Fisica dell'Università di Genova, via Dodecaneso 33, Genova 16146, Italy*

[‡]*Dipartimento di Fisica dell'Università di Genova and CNR-IMEM, via Dodecaneso 33, Genova 16146, Italy*

[¶]*Molecular Cryo-Electron Microscopy Unit, Okinawa Institute of Science and Technology Graduate University 1919-1 Tancha, Onna-son, Kunigami-gun Okinawa, Japan 904-0495*

[§]*Corresponding author*

E-mail: ferrando@fisica.unige.it; chloe.minnai@oist.jp

Abstract

The shape of AuPd nanoparticles is engineered by surface stress relaxation, achieved by varying the Au content in nanoparticles of Pd-rich compositions. AuPd nanoparticles are grown in the gas phase for several compositions and growth conditions. Their structure is atomically resolved by HRTEM/STEM and EDX. In pure Pd distributions the dominant structures are FCC truncated octahedra (TO), while increasing the Au content there is a transition to icosahedral (Ih) structures in which Au atoms are preferentially placed at the nanoparticle surface. The transition is sharper for growth conditions closer to equilibrium. The physical origin of the transition is determined with the aid of computer simulations. Global optimization searches and free energy calculations confirm that Ih become the equilibrium structure for increasing Au content. Atomic stress calculations demonstrate that the TO→Ih shape change is caused by a better relaxation of anisotropic surface stress in icosahedra.

Graphical TOC Entry

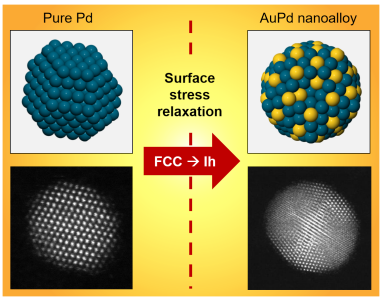

The fine details of atomic positions are often crucial in determining the properties of nanoparticles and their interactions with the environment. For example, surface strain [1] has a strong influence on the adsorption energy of atoms and molecules, with deep consequences for surface-catalyzed chemical reactions. [2–6]

In a strained nanoparticle, interatomic distances are either contracted or expanded with respect to the ideal lattice spacing of the bulk crystal. Strain is naturally present in non-crystallographic structures. In fact, in elemental icosahedral nanoparticles, interatomic distances are contracted in the central part and expanded at the surface. [7] Moreover, the environment around an atomic site of a nanoparticle is strongly anisotropic in many cases. As a consequence, strain can be anisotropic as well, and even of different types in different directions.

The presence of strain is associated to stress at the atomic level. [8] Contraction and expansion of distances correspond to compressive (positive) and tensile (negative) stress, respectively, and, in general, anisotropic strain generates anisotropic stress. Stress has an energetic cost, therefore its relaxation is beneficial to nanoparticle stability. From this line of reasoning, it follows that shape changes in nanoparticles might be obtained by using atomic stress to stabilize or destabilize specific structural motifs, as suggested in Ref. [9] on the basis of theoretical considerations concerning the relaxation of *internal stress*, i.e. in the inner part of a nanoparticle. The results reported here show that these stress-induced shape changes can indeed be experimentally achieved. At variance with Ref., [9] here we consider a case in which *surface stress* relaxation at the atomic level is the cause of the shape changes.

Specifically, in this Letter we demonstrate that the shape of AuPd nanoparticles can be controlled by varying the Au content in nanoparticles of Pd-rich compositions. We experimentally show that the substitution of a relatively modest proportion of Pd atoms in pure Pd nanoparticles by Au atoms causes a quite sharp shape change in the population of grown samples, from FCC truncated octahedral (TO) structures to icosahedral (Ih) ones. This morphology transition is obtained by growing the AuPd nanoparticles in the gas phase,

a method which takes advantage of a very clean growth environment. This allows a clear analysis of the key physical driving forces causing the transition, which are determined with the aid of computer simulations. In particular, our global optimization searches and free energy calculations find that Au atoms are preferentially placed at the nanoparticle surfaces, as experimentally confirmed by our EDX spectra. Moreover, the calculation of the atomic-level stress shows that surface Au atoms produce a much more efficient stress relaxation in the surfaces of icosahedra than in those of FCC truncated octahedra, especially for the stress components lying in the surface plane. This better stress relaxation is associated to an energy gain of icosahedra with respect to truncated octahedra, causing the TO→Ih shape change for increasing Au content.

AuPd nanoparticles are the subject of intense research activity,[10–17] mainly for their applications to catalysis, since they have been found to enhance reactivity in several chemical reactions, from the acetoxylation of ethylene to vinyl acetate, to alkene epoxidation, alcohol oxidation, aerobic glucose oxidation, Suzuki-Miyaura cross coupling and many others. For these reactions, the fine details of the arrangement of the two species in the nanoparticle surface are often of great importance,[14] as well as the nanoparticle geometric shape. In fact, it was shown that Ih and FCC nanoparticles can present quite different catalytic properties, as in the aerobic oxidation of cyclohexane, in which Ih nanoalloys presented a turnover frequency larger by three times than FCC octahedra.[16]

In our work, AuPd nanoparticles were synthesized by inert gas-aggregation sputtering deposition. This technique is based on the condensation of an atomic vapor produced by DC simultaneous magnetron-sputtering of Pd and Au targets, see Supporting Information (SI) for details. The applied powers were varied to obtain different compositions of the metal vapor, from pure Pd to three Pd-rich compositions: $Au_{15}Pd_{85}$, $Au_{25}Pd_{75}$, $Au_{35}Pd_{65}$. These values indicate the effective composition of the distributions of nanoparticles deposited on the substrates, and were quantitatively measured by performing EDX mapping on several frames of multiple samples fabricated in the same conditions. More details are reported in

the SI.

For each composition, a series of different experiments was made, corresponding to different residence times of the clusters in the aggregation zone. The residence time can be increased both by increasing the length of the aggregation zone (L_{AZ}) and by decreasing the pressure difference ΔP between the source and the deposition chamber (P_{DC}). Five growing conditions were tested: L_{AZ} = 45, 70, 95 and 125 mm with $P_{DC} = 6 \times 10^{-4}$ mbar and L_{AZ} = 125 mm with $P_{DC} = 4 \times 10^{-3}$ mbar. These growth conditions were chosen to avoid coalescence phenomena which would render the analysis of the origin of the final structures much more complicated.[18] The resulting clusters are deposited on carbon grids and then characterized by aberration-corrected HRTEM/STEM and by EDX.

A representative distribution of AuPd nanoparticles is presented in Figure S1. The HAADF/STEM analysis allowed to identify most structures in the sample, distinguishing three different structural motifs: crystalline FCC TO, and non-crystalline Ih and decahedra (Dh). Some examples of these structures are shown in Figure 1(a-d). For each composition and growth conditions, a number of nanoparticles between 80 and 150 was analyzed. Since in all samples the number of Dh structures was always much smaller than that of TO or Ih (see Figure S2 for complete data), in the following we focus on the analysis of the abundances of TO and Ih structures. The quantity %Icosahedra will indicate the percentage of Ih with respect to the sum of Ih and TO structures.

Let us analyze first how the relative abundance %Icosahedra evolves as a function of composition. The data are reported in Figure 1(e) for the five different growth conditions. In pure Pd distributions TO are by far dominant over Ih, being always between 5 and 20 times more abundant. But by increasing the Au content, Ih are observed more and more frequently, to reach a maximum abundance for composition $Au_{25}Pd_{75}$, where, depending on the growth conditions, Ih can be up to four times more abundant than TO. A further increase of the Au content to $Au_{35}Pd_{65}$ causes on average some decrease of %Icosahedra. At this composition, also the number of Dh structures is somewhat increased (see Figure

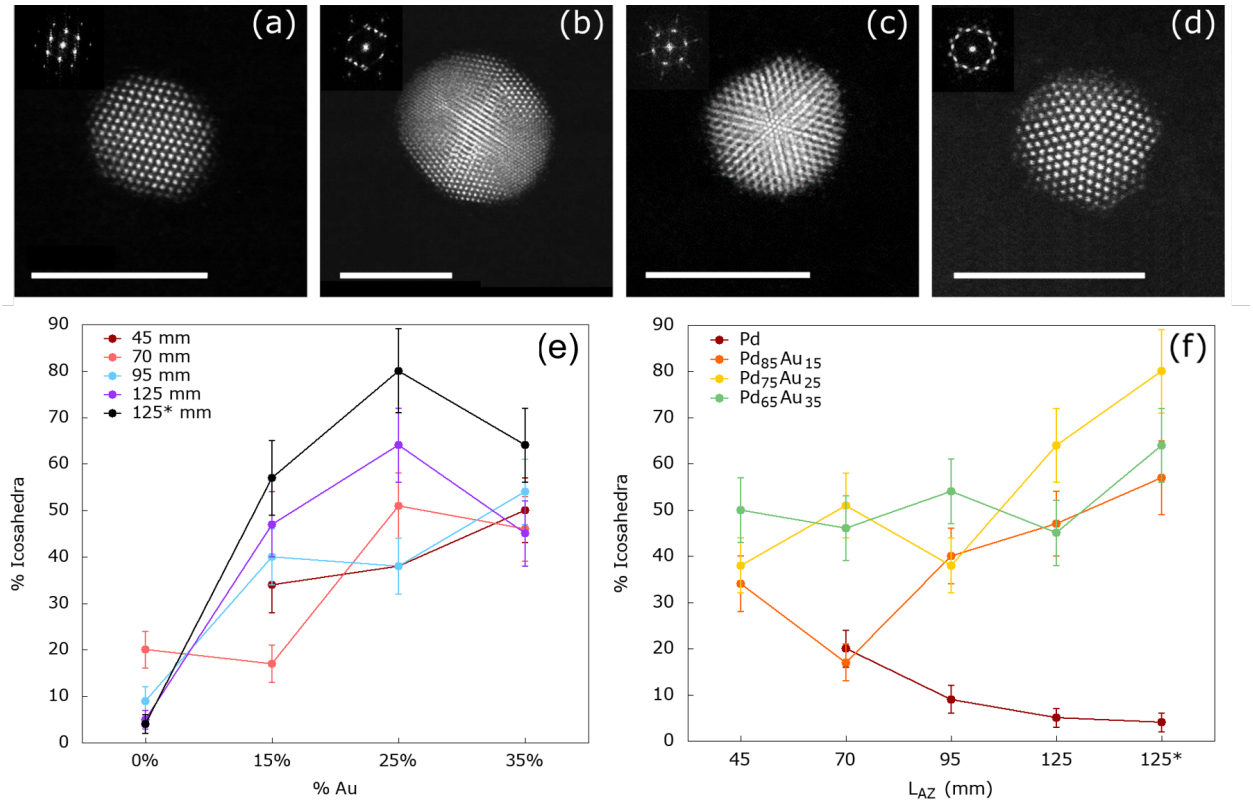

Figure 1: (a)-(d) Atomic-resolution HAADF–STEM image of AuPd nanoparticles with corresponding FFT data in the inset. The scale bar is of 5 nm. (a) Truncated-octahedral FCC nanoparticle; (b) and (c) icosahedral particles oriented with a three- and two-fold axis parallel to the electron beam, respectively; (d) decahedral nanoparticle along its five-fold symmetry axis. The five twin boundaries join at the center of the nanoparticle in (d). (e) Evolution of the percentage of AuPd icosahedral nanoparticles (%Icosahedra) on the total of Ih+fcc structures, as a function of the chemical composition of the distribution. Each curve refers to a different growth condition. The legend indicates the length of the aggregation zone (L_{AZ}) at which the distribution is grown. The pressure in the deposition chamber is P_{DC} = 6x10^{-4} mbar for the first four curves and P_{DC} = 7x10^{-3} mbar in the last one. (f) Evolution of %Icosahedra as a function of L_{AZ}. P_{DC}= 6x10^{-4} mbar for the first four L_{AZ} values and 7x10^{-3} mbar for the last point marked as "125* mm". Note that (e) and (f) show the same data set plotted in two different ways to show the effect of changing the chemical composition at fixed growth conditions (in (e)), and to show the effect of changing the growth conditions at fixed composition (in (f)).

S2(d)).

In Figure 1(f), we report %Icosahedra as a function of the growth conditions at fixed composition. By increasing L_{AZ} from 45 and 125 mm, and then decreasing ΔP at L_{AZ}=125 mm, one gradually increases the dwell time in the aggregation zone, so that the growth becomes closer and closer to thermodynamic equilibrium conditions, because the growing nanoparticles have more time to rearrange towards equilibrium structures during their growth.[19] Two different types of behaviours are visible in Figure 1(f). For pure Pd distributions, %Icosahedra decreases when growth becomes closer to equilibrium. On the contrary, for the distributions containing Au atoms, %Icosahedra tends to increase when going towards equilibrium. These results indicate that the dominance of TO over Ih in pure Pd and the opposite dominance of Ih over TO, which is especially evident for $Au_{25}Pd_{75}$, are likely to be related, at least to some extent, to the thermodynamic equilibrium abundances of these structural motifs. This point will be discussed in the following with the aid of computer simulations.

A further important aspect of the experimental characterization of our samples is the determination of nanoparticle chemical ordering. Au and Pd are known to present a strong tendency towards intermixing in their bulk equilibrium phase diagram.[20] In nanoparticles, equilibrium chemical ordering is expected to be influenced also by the tendency of Au to some degree of surface segregation, as found by several simulations results, including calculations using atomistic interaction potentials and density functional theory (DFT).[21–23] The tendency of surface placement of Au was observed in AuPd TO nanoparticles growth by wet-chemistry techniques.[14] Our EDX characterization of the grown nanoparticles is reported in Figure 2. An overall inspection of the samples by EDX (see the images in Figure 2(a,b) which show portions of a sample at different magnifications) unambiguously demonstrates that true AuPd nanoalloys are grown, without evidence for the formation of separated Au and Pd elemental nanoparticles. In addition, the EDX results confirm that the external part of AuPd nanoalloys is enriched in Au, for both Ih and FCC structures, as shown in Figure

2(c-e) and (f-h), respectively.

In summary our experimental results show that a quite sharp TO→Ih transition takes place because of the replacement of a relatively modest proportion of Pd atoms with Au atoms, with the Au atoms preferentially distributed in the nanoparticle shell. The TO→Ih transition becomes more evident when growth is closer to equilibrium.

What are the atomic-level driving forces of the TO→Ih transition? In order to answer to this question, here below we report the results of the computational analysis of equilibrium free energies and of atomic stress.

In order to determine whether Ih or TO structures are favorable at equilibrium, we performed global optimization searches and calculated free energy differences by the harmonic superposition approximation (HSA).[8,24] The nanoparticles were modeled by a force field of the second-moment tight-binding type[25–27] taken from Ref.[21] Details about the optimization procedure and the interaction potential are given in the SI. Here we note that this approach is the only available at present which allows a thorough exploration of the energy landscape, including crystalline, non-crystalline and defective structures, for sizes of several hundred atoms. For pure Pd clusters, for which some structures are precisely determined by the experiments,[28,29] our force field correctly predicts that the most favorable structure at 55 atoms is icosahedral, and that for size 147 Ih and TO are in close competition, with some prevalence for the TO. On the other hand, the interaction potential predicts that Dh would be in close competition with TO structures, therefore somewhat overestimating Dh stability.

Let us consider a local minimum s, which corresponds to a locally stable structure. In the HSA, its free energy F_s is given by the sum of translational, symmetry, vibrational and rotational contributions added to the energy E_s of the potential well bottom[8]

$$F_s = E_s + F_{tr,s} + F_{sym,s} + F_{vib,s} + F_{rot,s}. \quad (1)$$

The translational term $F_{tr,s}$ does not depend on the structure, so that it cancels in free

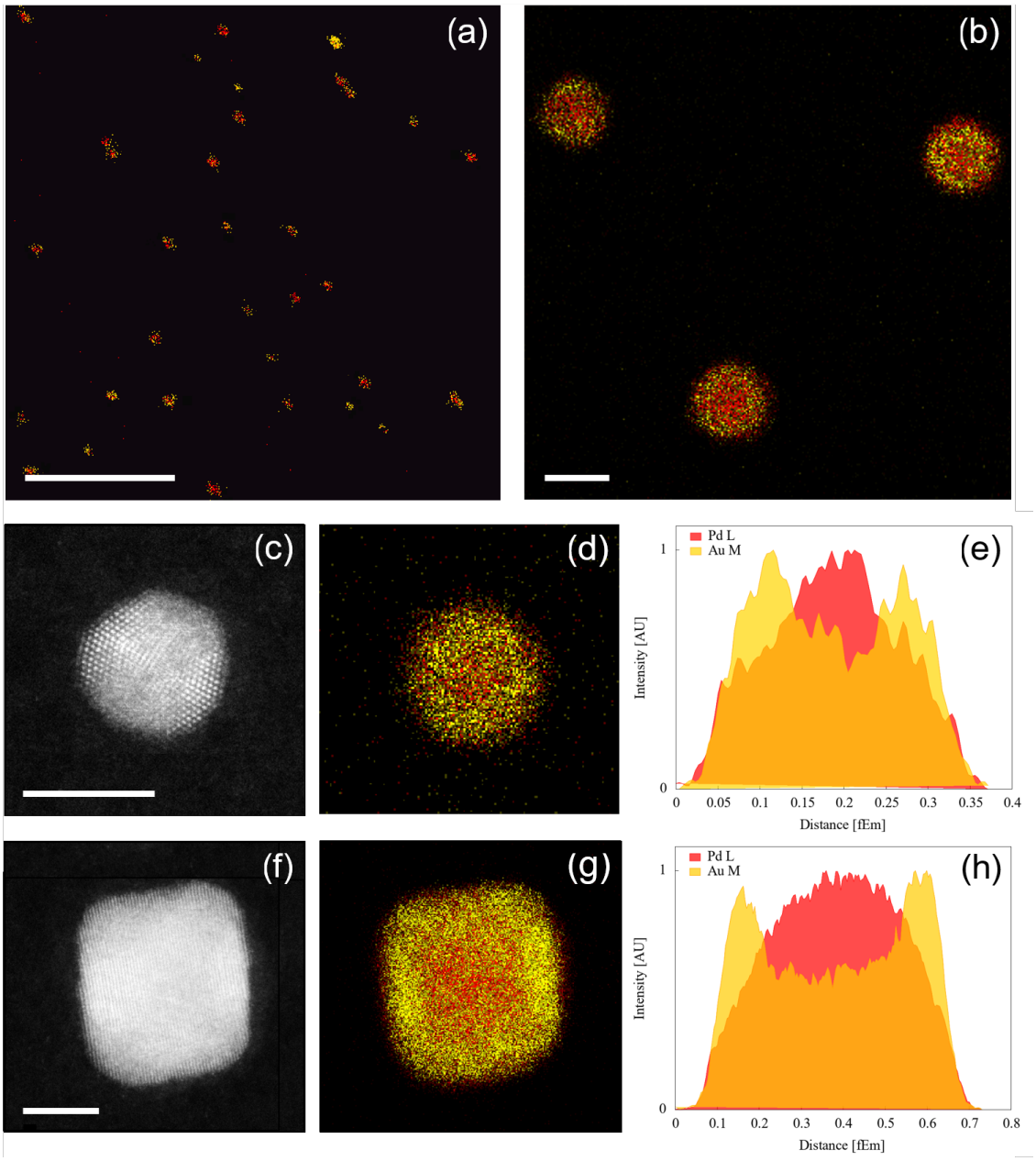

Figure 2: Elemental mapping of $Au_{25}Pd_{75}$ nanoparticles at different magnifications. The colors are based on the chemical composition of the nanoparticles where Au is in yellow and Pd in red. (a) Low magnification mapping showing that all the particles have a mixed composition. The size distribution is 3.9 ± 0.6 nm. Scale bar 50 nm. (b) Higher magnification mapping showing that the Au tend to enrich the surface of the particles. Scale bar 5 nm. The corresponding HAADF-STEM images are shown in Figure S1. $C_s$corrected HAADF-STEM images of AuPd particle with icosahedral (c) and truncated octahedral (f) structure. The elemental mapping acquired on the same particles (d,g) and the composition profiles (e,h), clearly show that Au atoms distribute at the surface of the particles. Scale bars 5 nm

energy differences. The other terms are given by

$$\begin{aligned} F_{sym,s} &= k_B T \ln(h_s) \\ F_{vib,s} &= k_B T \sum_{i=1}^{3N-6} \ln\left(2\sinh\left(\frac{\hbar\omega_{i,s}}{2k_B T}\right)\right) \\ F_{rot,s} &= -\frac{3}{2} k_B T \ln\left(\frac{2\pi k_B T \overline{I}_s}{\hbar^2}\right), \end{aligned} \tag{2}$$

where h_s is the order of the symmetry group, $\omega_{i,s}$ are the non-zero normal-mode frequencies, and $\overline{I}_s$ is the geometric average of the principal inertia moments. We considered four nanoparticle sizes ($N = 150, 200, 250, 300$). For each size, we calculated the free energy difference $\Delta F = F_{Ih} - F_{TO}$ between the best Ih and the best TO structure for different Pd-rich compositions at different temperatures. Representative images of the best Ih and TO structures are given in Figures S3 and S4, where it can be seen that Au atoms occupy surface sites, in agreement with our experiments and other results in the literature.[14,22] The ΔF results are reported in Figure 3. ΔF is always positive in pure Pd nanoparticles, reflecting the stronger stability of TO structures with respect to Ih ones. But at increasing Au content, ΔF becomes negative, showing a transition to Ih structures. This effect is very strong for $N = 150$ and $N = 300$, which are close to magic Ih sizes (147 and 309), whereas it is still present but weaker for $N = 200$, which is very close to the magic TO size 201. On the other hand, for $N = 250$, which is far from all magic sizes, the effect is quite strong too. Results for larger AuPd nanoalloys (size 561) can be found in Figure S6, showing that the TO→Ih transition is still present.

These results therefore show that Ih structures become energetically favorable in Pd-rich AuPd nanoalloys (see the results for $T = 0$ K) and that entropic contributions, mainly due to the vibrational term, tend to further stabilize Ih structures for increasing temperature. This confirms that the experimentally observed transition is mainly caused by thermodynamic equilibrium driving forces.

The question which arises from these results is: why Ih structures become energetically

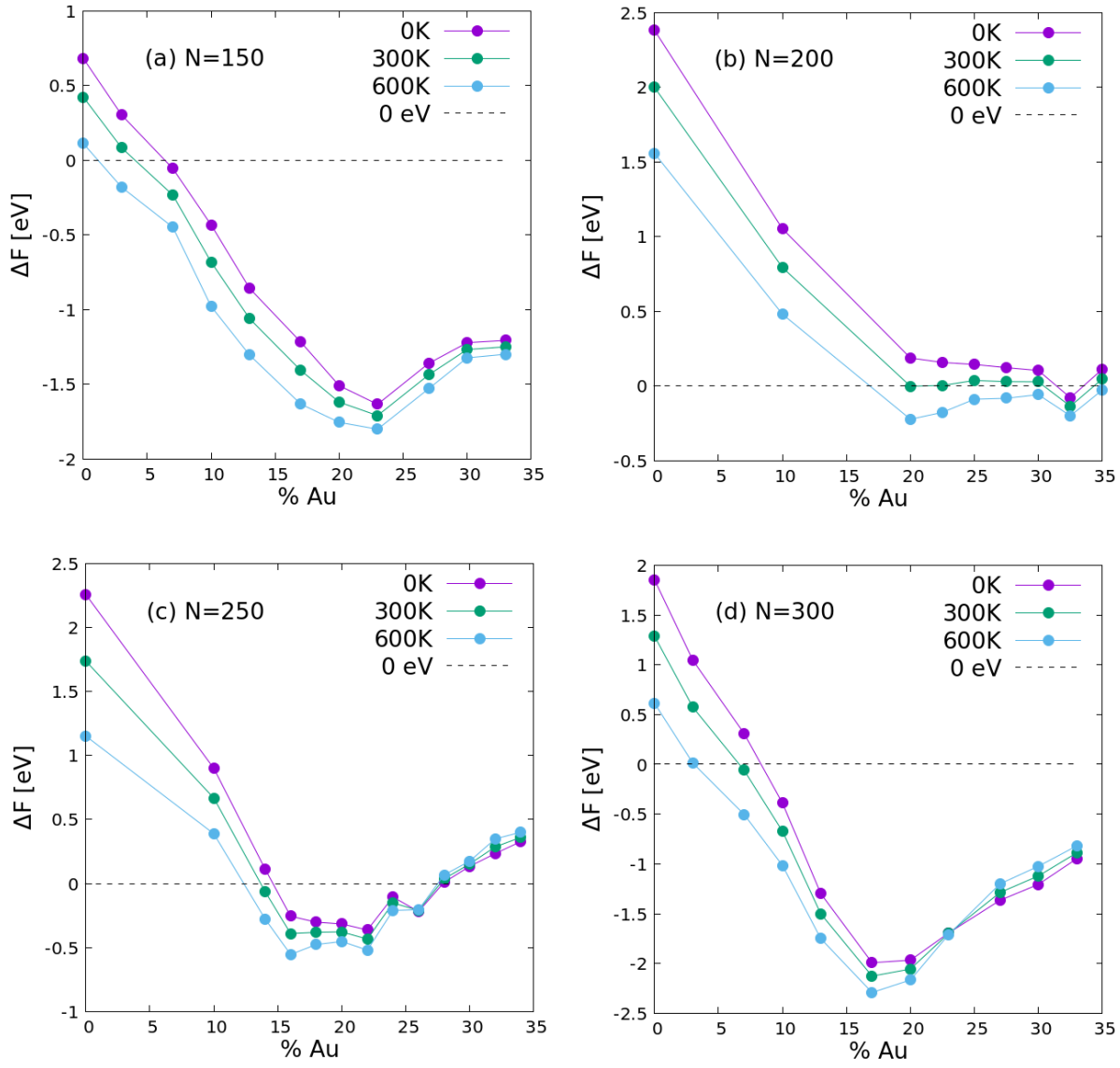

Figure 3: Free energy differences $\Delta F = F_{Ih} - F_{TO}$ between the best Ih and TO structures for different sizes and Pd-rich compositions. For $\Delta F < 0$ the Ih is favored over the TO at the thermodynamic equilibrium, while for $\Delta F < 0$ the opposite holds.

favorable when replacing surface Pd atoms with Au atoms? Our analysis will show that the relaxation of atomic stress is the key to understand this point.

The atomic stress tensor on atom i is given by[30]

$$\sigma_i^{ab} = -\frac{1}{3V_i} \sum_{j \neq i} \frac{\partial E_i}{\partial r_{ij}} \frac{r_{ij}^a r_{ij}^b}{r_{ij}} \tag{3}$$

with $a, b = x, y, z$, E_i and V_i energy and volume of the i-th atom, and r_{ij} distance between atoms i and j. This symmetric 3×3 matrix can be diagonalized, to find the principal stress components $p_{i,k}$ $(k = 1, 2, 3)$ whose sum gives the isotropically averaged atomic pressure. In the following we consider atoms placed in the surface sites of Ih and TO nanoparticles, as those shown in Figure 4a and 4b, respectively. For these atoms, one component (p_r in the following) lies approximately in radial direction, while the other two components are transverse, lying close to the surface plane for terrace sites. In the following p_t indicates the arithmetic mean of the transverse components.

The results for atoms in the sites of Figure 4 are given in Table 1. For pure Pd nanoparticles, all stress components are negative, corresponding to tensile stress in all directions. The absolute magnitude of the tensile stress is considerably larger in the Ih than in the FCC TO nanoparticle, especially for terrace sites and some edge sites, due to the expanded distances in the (111)-like Ih surfaces compared to ideal (111) surfaces. When a Pd atom is replaced by a larger atom like Au, the strong tensile stress in the Ih relaxes very well, especially in terrace sites where all stress components get close to zero: the sum of the moduli $|p_r| + 2|p_t|$ decreases from about 8 GPa to less than 1 GPa. On the contrary, in the TO structure, the Au impurity well relaxes only the radial component p_r, while the components in the surface plane become strongly positive, so that $|p_r| + 2|p_t|$ increases from 2-4 to 6-8 GPa. For this reason, the energy gain due to the impurity is considerably larger in Ih terraces than in FCC(111) terraces. We note that in the FCC TO structure, placement of Au atoms is more favorable at edges and vertices than on (111) terraces, in agreement with experimental ob-

servations and DFT calculations,[14,22] while in the Ih terrace sites are slightly more favorable. The difference in energy gain of Au impurities in (111) terraces between Ih and TO tends to become slightly larger for larger nanoparticle sizes. In summary, these results show that the replacement of Pd atoms with Au atoms in surface sites is more effective in the Ih, so that after replacing a sufficient number of atoms the Ih structure becomes energetically favorable against the TO (and also against Dh structures, as shown in Figure S5).

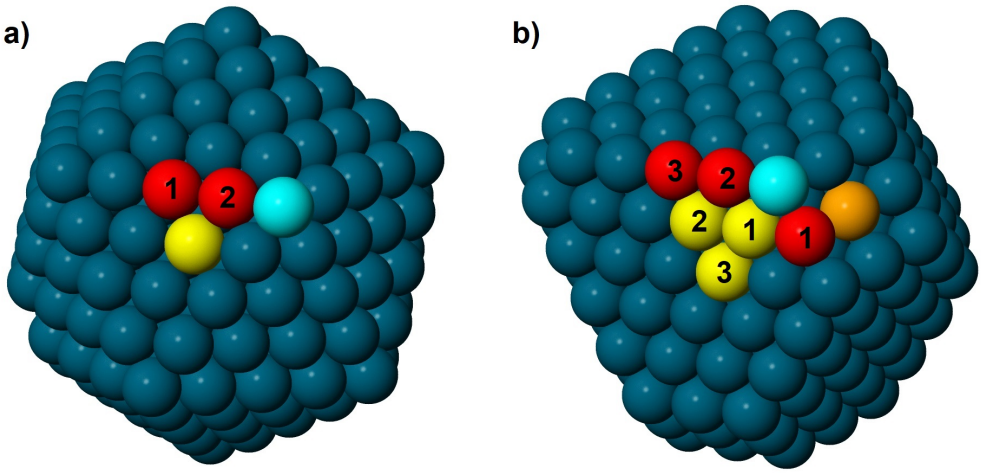

Figure 4: Sites at which Pd atoms are replaced by Au atoms in (a) the best 300-atom pure Pd Ih and (b) the best 300-atom pure Pd TO. Vertex sites are in cyan, edge sites in red, (111)-terrace sites in yellow and (100)-terrace sites in orange. In these sites the data of Table 1 are calculated.

Our analysis therefore indicates that the main driving force for the TO→Ih shape change derives from the equilibrium energetics for varying composition. However, in nanoparticle growth, kinetic effects are usually expected to occur to some extent.[7] Therefore, our finally observed nanoparticles may in principle present some form of kinetic trapping, because the time scale for attaining equilibrium becomes longer and longer as a nanoparticle grows in size, so that it may happen that the growing nanoparticles equilibrate up to some critical size (in our case of at least 2-3 nm, likely larger) and then they grow by a kind of *template growth*.[31] In template growth, the geometric structure is selected in the first part of the growth (in which equilibrium shapes are formed) and then preserved as the nanoparticle grows further. This point is currently under investigation.

Table 1: Replacement of Pd Atoms with Au Atoms on Ih and FCC Surface Sites: Energy Gain (ΔE) and Effect on the Radial and Transverse Strain Components (p_r and p_t)

structure	site	ΔE	bonds	p_r		p_t		$\lvert p_r \rvert + 2\lvert p_t \rvert$		
				Pd[a]	Au[b]	Pd	Au	Pd	Au	Δ[c]
IH	111	-0.537	9	-4.13	-0.12	-1.90	0.25	7.93	0.62	-7.31
	edge_1	-0.518	8	-4.31	-1.16	-1.83	-0.02	7.97	1.20	-6.77
	edge_2	-0.510	8	-3.25	-0.54	-1.47	0.67	6.19	1.88	-4.31
	vertex	-0.448	6	-2.19	-0.65	-1.39	0.05	4.97	0.75	-4.22
FCC	111_1	-0.411	9	-1.07	0.15	-0.46	4.01	1.99	8.17	6.18
	111_2	-0.402	9	-1.19	0.18	-0.86	3.53	2.91	7.24	4.33
	111_3	-0.384	9	-1.77	0.16	-1.13	2.99	4.03	6.14	2.11
	100	-0.459	8	-2.04	-0.40	-1.57	0.71	5.18	1.82	-3.36
	edge_1	-0.457	7	-2.16	-0.48	-1.46	0.45	5.08	1.38	-3.70
	edge_2	-0.453	7	-2.45	0.02	-1.17	0.57	4.79	1.16	-3.63
	edge_3	-0.448	7	-2.65	0.07	-1.18	0.46	5.01	0.99	-4.02
	vertex	-0.441	6	-2.22	-0.50	-1.41	-0.04	5.04	0.58	-4.46

Notes: values refer to the sites of Figure 4; energies are in eV and stress values in GPa
[a]stress values for the atomic sites in the pure Pd nanoparticle
[b]stress values after replacing the Pd atom with an Au atom
[c]variation due to the replacement

In conclusion our results show that atomic-level stress can be used to induce shape changes in nanoparticles, by either stabilizing or destabilizing specific structural types. In AuPd, the size mismatch between the larger Au atoms and the smaller Pd atoms is used to very well relax the tensile stress of the expanded surfaces of Ih nanoparticles, while size mismatch induces a less efficient relaxation in the surfaces of FCC TO nanoparticles because of compressive stress in the terrace planes. We believe that simple physical mechanisms of this type can be effective for a wide class of binary and of ternary systems, for both gas phase and wet chemistry synthesis methods. This opens up very interesting perspectives in the fast developing fields of nanoparticle structure engineering and controlled growth,[32,33] with foreseeable huge impact on their applications.

Acknowledgement

The research performed at OIST was supported by funding from the Okinawa Institute of Science and Technology Graduate University. We thank OIST Imaging Section for provide access to JEOL JEM-ARM200F and for their support. The authors acknowledge networking support from the International Research Network Nanoalloys of CNRS.

Supporting Information

The Supporting Information is available free of charge at https://pubs.acs.org/

Experimental methods

Experimental data on the distribution of the different structural motifs

Global Optimization results

Free energy differences between Ih and Dh

Global optimization for size 561

Author contributions

All experiments were conducted by CM. Experimental structures were analyzed by CM and DN. Global optimization searches were made by DN. Free energy calculations were made by CR and RF. Atomic stress calculations were made by DN and RF. All authors contributed to writing the manuscript.

References

(1) Yang, S.; Liu, F.; Wu, C.; Yang, S. Tuning Surface Properties of Low Dimensional Materials via Strain Engineering. *Small* **2016**, *12*, 4028–4047.

(2) Mavrikakis, M.; Hammer, B.; Nørskov, J. K. Effect of Strain on the Reactivity of Metal Surfaces. *Phys. Rev. Lett.* **1998**, *81*, 2819–2822.

(3) Wu, J.; Li, P.; Pan, Y.-T. F.; Warren, S.; Yin, X.; Yang, H. Surface Lattice-Engineered Bimetallic Nanoparticles and Their Catalytic Properties. *Chem. Soc. Rev.* **2012**, *41*, 8066–8074.

(4) Alayoglu, S.; Nilekar, A. U.; Mavrikakis, M.; Eichhorn, B. Ru-Pt Core-Shell Nanoparticles for Preferential Oxidation of Carbon Monoxide in Hydrogen. *Nature Mater.* **2008**, *7*, 333–338.

(5) Alayoglu, S.; Zavalij, P.; Eichhorn, B.; Wang, Q.; Frenkel, A. I.; Chupas, P. Structural and Architectural Evaluation of Bimetallic Nanoparticles: A Case Study of Pt-Ru Core-Shell and Alloy Nanoparticles. *ACS Nano* **2009**, 3127–3137.

(6) Tao, F.; Grass, M. E.; Zhang, Y.; Butcher, D. R.; Aksoy, F.; Aloni, S.; Altoe, V.; Alayoglu, S.; Renzas, J. R.; Tsung, C.-K.; *et. al.*, Evolution of Structure and Chemistry of Bimetallic Nanoparticle Catalysts under Reaction Conditions. *J. Am. Chem. Soc.* **2010**, *132*, 8697–8703.

(7) Baletto, F.; Ferrando, R. Structural Properties of Nanoclusters: Energetic, Thermodynamic, and Kinetic Effects. *Rev. Mod. Phys.* **2005**, *77*, 371–423.

(8) Ferrando, R. *Structure and Properties of Nanoalloys*; Frontiers of Nanoscience, Volume 10; Elsevier, 2016.

(9) Panizon, E.; Bochicchio, D.; Rossi, G.; Ferrando, R. Tuning the Structure of Nanoparticles by Small Concentrations of Impurities. *Chem. Mater* **2014**, *26*, 3354–3356.

(10) Ferrer, D.; Torres-Castro, A.; Gao, X.; Sepúlveda-Guzmán, S.; Ortiz-Méndez, U.; José-Yacamán, M. Three-Layer Core/Shell Structure in Au-Pd Bimetallic Nanoparticles. *Nano Lett.* **2007**, *7*, 1701–1706.

(11) Hutchings, G. J. Nanocrystalline Gold and Gold Palladium Alloy Catalysts for Chemical Synthesis. *Chem. Commun.* **2008**, 1148–1164.

(12) Mariscal, M. M.; Mayoral, A.; Olmos-Asar, J. A.; Magen, C.; Mejía-Rosales, S.; Pérez-Tijerina, E.; José-Yacamán, M. Nanoalloying in Real Time. A High Resolution STEM and Computer Simulation Study. *Nanoscale* **2011**, *3*, 5013–5019.

(13) Chen, M.; Kumar, D.; Yi, C.-W.; Goodman, D. W. The Promotional Effect of Gold in Catalysis by Palladium-Gold. *Science* **2005**, *310*, 291–293.

(14) Zhang, H.; Watanabe, T.; Okumura, M.; Haruta, M.; Toshima, N. Catalytically Highly Active Top Gold Atom on Palladium Nanocluster. *Nature Materials* **2012**, *11*, 49–52.

(15) Sarina, S.; Zhu, H.; Jaatinen, E.; Xiao, Q.; Liu, H.; Jia, J.; Chen, C.; Zhao, J. Enhancing Catalytic Performance of Palladium in Gold and Palladium Alloy Nanoparticles for Organic Synthesis Reactions through Visible Light Irradiation at Ambient Temperatures. *Journal of the American Chemical Society* **2013**, *135*, 5793–5801, PMID: 23566035.

(16) Wang, L.; Zhao, S.; Liu, C.; Li, C.; Li, X.; Li, H.; Wang, Y.; Ma, C.; Li, Z.; Zeng, J. Aerobic Oxidation of Cyclohexane on Catalysts Based on Twinned and Single-Crystal Au75Pd25 Bimetallic Nanocrystals. *Nano Letters* **2015**, *15*, 2875–2880, PMID: 25839191.

(17) Larios-Rodríguez, E. A.; Castillón-Barraza, F. F.; Herrera-Urbina, R.; Santiago, U.; Posada-Amarillas, A. Synthesis of AucorePdshell Nanoparticles by a Green Chemistry Method and Characterization by HAADF-STEM Imaging. *Journal of Cluster Science* **2017**, *28*, 2075–2086.

(18) Nelli, D.; Cerbelaud, M.; Ferrando, R.; Minnai, C. Tuning the Coalescence Degree in the Growth of Pt–Pd Nanoalloys. *Nanoscale Adv.* **2021**, –.

(19) Plant, S. R.; Cao, L.; Palmer, R. E. Atomic Structure Control of Size-Selected Gold Nanoclusters during Formation. *Journal of the American Chemical Society* **2014**, *136*, 7559–7562.

(20) Okamoto, H.; Massalski, T. B. The Au-Pd (Gold-Palladium) System. *Bull. Alloy Phase Diagrams* **1985**, *6*, 229–235.

(21) Pittaway, F.; Paz-Borbón, L. O.; Johnston, R. L.; Arslan, H.; Ferrando, R.; Mottet, C.; Barcaro, G.; Fortunelli, A. Theoretical Studies of Palladium-Gold Nanoclusters: Pd-Au Clusters with up to 50 Atoms. *The Journal of Physical Chemistry C* **2009**, *113*, 9141–9152.

(22) Kozlov, S. M.; Kovács, G.; Ferrando, R.; Neyman, K. M. How to Determine Accurate Chemical Ordering in Several Nanometer Large Bimetallic Crystallites from Electronic Structure Calculations. *Chem. Sci.* **2015**, *6*, 3868–3880.

(23) Kovács, G.; Kozlov, S. M.; Neyman, K. M. Versatile Optimization of Chemical Ordering in Bimetallic Nanoparticles. *The Journal of Physical Chemistry C* **2017**, *121*, 10803–10808.

(24) Doye, J. P. K.; Calvo, F. Entropic Effects on the Size Dependence of Cluster Structure. *Phys. Rev. Lett.* **2001**, *86*, 3570–3573.

(25) Cyrot-Lackmann, F.; Ducastelle, F. Binding Energies of Transition-Metal Atoms Adsorbed on a Transition Metal. *Phys. Rev. B* **1971**, *4*, 2406–2412.

(26) Gupta, R. P. Lattice Relaxation at a Metal Surface. *Phys. Rev. B* **1981**, *23*, 6265.

(27) Rosato, V.; Guillopé, M.; Legrand, B. Thermodynamical and Structural Properties of F.C.C. Transition Metals using a Simple Tight-Binding Model. *Phil. Mag. A* **1989**, *59*, 321.

(28) Rapps, T.; Ahlrichs, R.; Waldt, E.; Kappes, M. M.; Schooss, D. On the Structures of 55-Atom Transition-Metal Clusters and Their Relationship to the Crystalline Bulk. *Angewandte Chemie International Edition 52*, 6102–6105.

(29) Kohaut, S.; Rapps, T.; Fink, K.; Schooss, D. Structural Evolution of Palladium Clusters Pd55—Pd147–: Transition to the Bulk. *The Journal of Physical Chemistry A* **2019**, *123*, 10940–10946, PMID: 31769986.

(30) Vitek, V.; Egami, T. Atomic Level Stresses in Solids and Liquids. *Physica Status Solidi B* **1987**, *144*, 145–156.

(31) Wells, D. M.; Rossi, G.; Ferrando, R.; Palmer, R. E. Metastability of the Atomic Structures of Size-Selected Gold Nanoparticles. *Nanoscale* **2015**, *7*, 6498–6504.

(32) Baletto, F. Structural Properties of Sub-Nanometer Metallic Clusters. *Journal of Physics: Condensed Matter* **2019**, *31*, 113001.

(33) Fichthorn, K. A.; Yan, T. Shapes and Shape Transformations of Solution-Phase Metal Particles in the Sub-nanometer to Nanometer Size Range: Progress and Challenges. *The Journal of Physical Chemistry C* **2021**, *125*, 3668–3679.